International Journal of Nanomedicine Dovepress

Open Access Full Text Article ORIGINAL RESEARCH

Photo-Thermally Controllable Tumor Metabolic Modulation to Assist T Cell Activation for Boosting Immunotherapy

Jun Ma[1,*], Lixin Hua[2,*], Yinxing Zhu[3], Guangyao Mao[4], Chunsheng Fu[4], Shiyue Qin[5]

[1]General Surgery Department, Shanxi Bethune Hospital, Shanxi Academy of Medical Sciences, Third Hospital of Shanxi Medical University, Tongji Shanxi Hospital, Taiyuan, 030032, People's Republic of China; [2]Department of General Surgery, Affiliated Huishan Hospital of Xinglin College, Nantong University, Wuxi Huishan District People's Hospital, Wuxi, People's Republic of China; [3]Department of Traditional Chinese Medicines, Taizhou Affiliated Hospital of Nanjing University of Chinese Medicine, Taizhou, 225300, People's Republic of China; [4]Institute of Clinical Medicine, the Affiliated Taizhou People's Hospital of Nanjing Medical University, Taizhou School of Clinical Medicine, Nanjing Medical University, Taizhou, 225300, People's Republic of China; [5]Department of Ophthalmology, the Affiliated Taizhou People's Hospital of Nanjing Medical University, Taizhou School of Clinical Medicine, Nanjing Medical University, Taizhou, 225300, People's Republic of China

*These authors contributed equally to this work

Correspondence: Shiyue Qin, Email qinshiyue20230419@njmu.edu.cn

Background: Glycolysis is crucial for tumor cell proliferation, supporting their energy needs and influencing the tumor microenvironment (TME). On one hand, increased lactate levels produced by glycolysis acidifies the TME, inhibiting T cell activity. On the other hand, glycolysis promotes the expression of PD-L1 through various mechanisms, facilitating immune evasion. Therefore, controlled modulation of glycolysis in tumor cells to subsequently improve the immune tumor microenvironment holds significant implications for clinical cancer treatment and immune regulation.

Methods: To reverse the immunosuppressive microenvironment caused by tumor glycolysis and reduce tumor immune escape, we developed a photo-thermal-controlled precision drug delivery platform to regulate tumor metabolism and aid in the activation of T cells, thereby enhancing immunotherapy. First, hollow mesoporous Prussian blue (HPB) was prepared, and the glycolysis inhibitor 3-bromopyruvate (3-BrPA) was encapsulated within HPB using the phase-change material 1-tetradecanol, resulting in B/T-H. This product was then modified with tumor cell membranes to obtain a photo-thermal controllable regulator (B/T-H@Membrane, B/T-HM).

Results: Due to the excellent drug loading and photo-thermal properties of HPB, upon reaching the tumor, B/T-HM can rapidly heat under 808 nm irradiation, causing the 1-tetradecanol to transition to a liquid phase and release 3-BrPA, which effectively inhibits tumor glycolysis through the HK2 pathway, thereby reducing tumor cell proliferation, decreasing lactate production, and down-regulating tumor PD-L1 expression. In synergy with photo-thermal and αPD-1, this photo-thermally controllable metabolic-immune therapy effectively activates T cells to eliminate tumor.

Conclusion: In response to the changes in immune microenvironment caused by tumor metabolism, a photo-thermal precision-controlled drug delivery platform was successfully developed. This platform reshapes the tumor immunosuppressive microenvironment, providing a new approach for T cell-based tumor immunotherapy. It also opens new avenues for photo-thermal controllable metabolic-immune therapy.

Keywords: photo-thermally controllable, glycolysis, PD-L1, T cell, metabolic-immune therapy

Introduction

Cancer immunotherapy marks a transformative progress in oncology, principally focusing on activating or rejuvenating the patient's immune system to detect and eradicate tumor cells.[1–3] However, various immunosuppressive mechanisms within the tumor microenvironment (TME), including local immune suppression and impaired immune cell function, pose significant challenges to the efficacy of immunotherapy.[4–6] This indicates that a deep understanding and resolution of immune escape within the TME are crucial for the effectiveness of cancer immunotherapy.

Received: 22 June 2024
Accepted: 21 October 2024
Published: 3 November 2024

Glycolysis, as a key metabolic pathway for the rapid proliferation of tumor cells, not only satisfies their demands for energy and biosynthetic precursors, but also profoundly influences the TME.[7–10] The increase of lactate, the metabolic end-product of glycolysis, within tumor leads to the acidification of the TME.[11–13] This not only boosts the invasiveness and survival of tumor cells but also markedly inhibits the function of anti-tumor immune cells, including T cells, further encouraging the proliferation and persistence of tumor cells.[14–17] Moreover, the activity of key enzymes in the glycolysis process, such as hexokinase 2 (HK2), is associated with an increased expression of programmed death-ligand 1 (PD-L1) on tumor cells.[18–20] HK2 accelerates the glycolysis process, helping tumor cells rapidly utilize glucose, thereby supporting their energy needs and rapid proliferation.[21,22] Simultaneously, the enhanced expression of PD-L1 not only inhibits the attack by the immune system but also promotes tumor resistance to treatment.[2,23–26] Therefore, by precisely targeting key enzymes in the glycolytic metabolic pathway, such as HK2, it is possible to not only weaken the metabolic capacity of tumor cells but also enhance the activity of immune cells by modulating the TME.[27–29] This in turn boosts the efficacy of immunotherapeutic drugs, including immune checkpoint inhibitors, and their combination therapies.

Hollow mesoporous Prussian blue (HPB), due to its excellent photo-thermal conversion and drug loading capabilities, has shown great potential in cancer treatment and imaging.[30–36] Due to its unique hollow and mesoporous structure, HPB can efficiently encapsulate drugs and release them.[37–40] Furthermore, its inherent photo-thermal properties enable the conversion of near-infrared light into heat, thereby generating photo-thermal therapy (PTT) and inducing immunogenic cell death (ICD) in tumor cells.[41–44] 1-Tetradecanol is widely used in the biomedical field due to its good biocompatibility. It is a phase-change material exhibiting a phase transition temperature of 38°C, a characteristic that makes it highly suitable for precise control of drug release.[45,46] Therefore, constructing a photo-thermally controlled drug delivery platform based on HPB and 1-tetradecanol may enable precise targeting and modulation of tumor cells.

In this study, to reverse the tumor metabolism-mediated immunosuppressive microenvironment, reduce tumor immune escape, and activate T cell function to promote immunotherapy, we encapsulated the glycolysis inhibitor 3-BrPA into HPB using 1-tetradecanol and performed cell membrane modification (B/T-HM), constructing a precision drug delivery platform controlled by photo-thermal therapy to regulate tumor metabolism and assist in T cell activation to enhance immunotherapy (Scheme 1). In vitro, B/T-HM exhibited excellent photo-thermal performance and drug encapsulation capabilities, effectively raising the temperature and precisely releasing 3-BrPA under 808 nm light exposure. At the cellular level, B/T-HM was efficiently internalized by tumor cells, and post-illumination, it reduced HK2 expression and activity levels through glycolysis inhibition, decreased lactate production, and degraded tumor PD-L1, effectively killing tumor cells and releasing tumor-associated antigen (TAA) after combined photo-thermal therapy. In vivo, B/T-HM targetedly accumulated in tumors and significantly inhibited tumor proliferation and immunogenic death under controlled photo-thermal synergy. Importantly, the reduction in tumor PD-L1 and decreased lactate production created a favorable immune microenvironment for T cell infiltration and activation. With further enhancement of T cells by αPD-1, the B/T-HM-mediated photo-thermally controllable metabolic-immune therapy effectively eradicated tumors. Overall, this study precisely regulated tumor metabolism through photo-thermal therapy, reshaped the tumor immunosuppressive microenvironment, and opened new avenues for integrating photo-thermal, metabolic regulation, and immunotherapy.

Materials and Methods

Materials and Characterization

3-Bromopyruvic acid (3BrPA), 1-Tetradecanol, Potassium ferricyanide ($K_3FeC_6N_6$), polyvinylpyrrolidone K30 (PVP K-30) and hydrogen chloride (HCl) were obtained from Sigma-Aldrich. FITC and fluorescent reagents were obtained from Shandong Sparkjade Biotechnology Co., Ltd. The antibodies (HSP 70, HSP 90, CRT, PD-L1, HK2,) for Western blot and immunofluorescence staining were obtained from CST and Zen-bio. All additional reagents were sourced from local vendors and utilized without any subsequent purification. Morphological characterization was performed using a JEM-1011 transmission electron microscope. In vitro and in vivo analyses were performed using a flow cytometer (BD Accuri®C6), scanning confocal laser microscope (LSM900, Zeiss) and IVIS imaging system (Perkin Elmer).

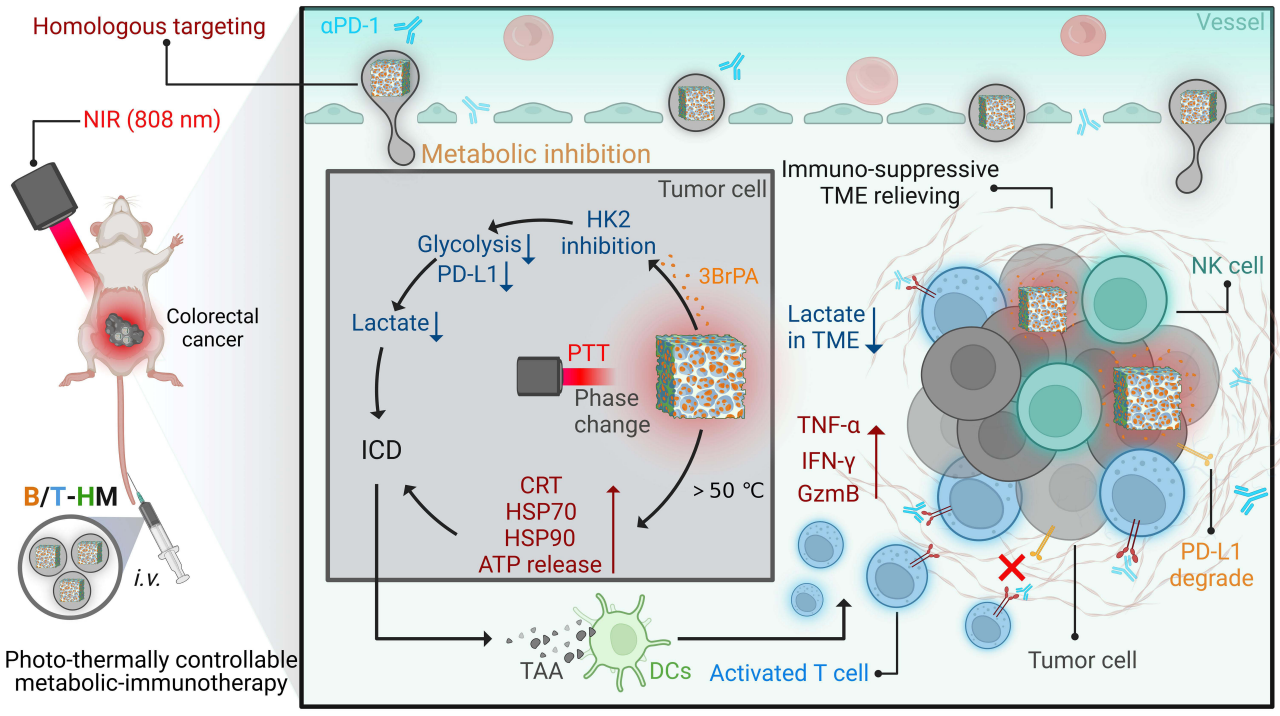

Scheme 1 Schematic diagram of photo-thermally controllable tumor metabolic modulation to assist T cell activation for boosting immunotherapy.

Cell Lines and Animals

CT26 colorectal cells, sourced from the Cell Source Center at the Chinese Academy of Science in Shanghai, China, were cultured under standard laboratory conditions. Female BALB/c mice (6–8 w) were procured from the Beijing Vital River Laboratory Animal Technology Co., Ltd. All animal experiments adhered to the ethical standards established by the Laboratory Animal Center at Nanjing Medical University. To establish a subcutaneous tumor model, mice were injected subcutaneously with $2*10^6$ CT26 cells suspended in approximately 25 μL of PBS on their dorsum. Tumor sizes were determined using the equation: Tumor volume=$0.5*length*width^2$.

Synthesis of B/T-HM

Hollow mesoporous Prussian blue nanoparticles (HPB) were produced using a standard procedure. Initially, to create Prussian blue nanoparticles (PB), $K_3[Fe(CN)_6$ (260 mg) and PVP K-30 (6 g) were dissolved in a 0.01 M HCl solution (60 mL). This mixture was then heated for 24 h in a reaction vessel. In the next step, the obtained PB nanoparticles (25 mg) were combined with additional PVP K-30 (75 mg) and dissolved in a stronger HCl solution (1 M, 20 mL). This mixture was left to etch in the reaction vessel at 140 °C for 2 h. Finally, the resulting product was washed with water and centrifuged to isolate the HPB.

To load 3BrPA and 1-Tetradecanol into HPB, 100 mg of 3BrPA is mixed with 100 mg of 1-Tetradecanol and heated to 85 °C to transform it from solid to liquid. Afterwards, 50 mg of HPB (dispersed in methanol) is added and mixed evenly under heated stirring conditions. Methanol is removed by evaporation, followed by the addition of 10 mL of hot deionized water (85 °C) to the suspension. The HPB loaded with 3BrPA and 1-Tetradecanol is collected by centrifugation (14000 rpm). Meanwhile, it is washed with room temperature deionized water (25 °C) to solidify 1-Tetradecanol, obtaining HPB encapsulated with 3BrPA and 1-Tetradecanol (B/T-HPB), yield 26.4±1.95%. Finally, B/T-HPB (0.5 mg/mL, 2 mL) is mixed with tumor cell membranes (1 mg/mL, 1 mL) and processed using a liposome extruder with an extrusion pore size of 400 nm to obtain B/T-HM.[40,47]

In vitro Controlled Release of 3BrPA from B/T-HM

The B/T-HM obtained was redispersed into dialysis bags (MWCO 8~14k Da) containing PBS (100 μg/mL, 5 parallel samples), which were then maintained at 37 °C with shaking for 5 minutes. Following this, the solutions underwent

irradiation with 808 nm NIR for 5 minutes (0.5 W/cm^2). At predetermined time intervals, the external solution was collected and lyophilized. The cumulative release of 3BrPA was quantified using HPLC.

In vitro Cellular Experiments

For uptake experiments, FITC-labeled B/T-HM nanoparticles (100 μg/mL) were co-incubated with CT26 cells for various durations, followed by fixation and staining with DAPI. Subsequently, results were acquired through scanning confocal laser microscope (LSM900, Zeiss).

To evaluate the biosafety of T-HM, HUVEC cells were pre-seeded in a 96-well plate (5000 cells/well). After 12 h, different concentrations of T-HM (0~200 μg/mL) were introduced and co-incubated for 24 h and then assessed using the CCK-8 assay kit.

To evaluate the cytotoxicity of B/T-HM on tumor cells under NIR control, CT26 cells were pre-seeded in a 96-well plate at a density of 5000 cells per well. After 12 h, the cells were treated with various conditions: Ctrl, NIR, B/T-HM, T-HM+NIR, and B/T-HM+NIR (B/T-HM at 100 μg/mL, 3BrPA at 25 μg/mL, NIR at 0.5 W/cm^2). The cells were then incubated for an additional 24 h. Cell viability was assessed by CCK-8 assay kit.

For Western blot (WB) analysis, CT26 cells pre-seeded in 6-well plates (2*10^6 cells/well) were treated with Ctrl, NIR, B/T-HM, T-HM+NIR, and B/T-HM+NIR (B/T-HM: 100 μg/mL, 3BrPA: 25 μg/mL, NIR: 0.5 w/cm^2). Subsequently, cells within 6-well plates underwent lysis at 0 °C with lysis buffer for protein extraction and sample preparation. Protein alterations, specifically in HK2, PD-L1, HSP70, and HSP90, were then discerned via gel electrophoresis and subsequent antibody identification, culminating in a process for visualizing the proteins.

To detect ATP content ion, CT26 cells, pre-seeded in 6-well plates at a density of 5*10^6 cells/well, were subjected to treatments with Ctrl, NIR, B/T-HM, T-HM+NIR, and B/T-HM+NIR (B/T-HM: 100 μg/mL, 3BrPA: 25 μg/mL, NIR: 0.5 w/cm^2). Subsequently, the cell culture medium was extracted and analyzed for ATP content using an ATP assay kit.

In vivo Experiments

For IVIS imaging, CT26 tumor-bearing BALB/c mice were intravenously (*i.v.*) injected with DiD-labeled B/T-HM (250 μL, 2 mg/mL, 3-BrPA: 0.5 mg/mL). Subsequently, fluorescence imaging was conducted at various time intervals through IVIS imaging system. After the imaging sessions, the mice were euthanized to harvest organs and tumors, which were then subjected to digestion using aqua regia. Finally, the content of B/T-HM in the organs and tumor was quantified using ICP-OES to assess its bio-distribution.

To acquire photo-thermal imaging, CT26 tumor-bearing BALB/c mice were *i.v.* injected with B/T-HM (250 μL, 2 mg/mL, 3BrPA: 0.5 mg/mL), which were then irradiated with NIR (0.5 w/cm^2), and photo-thermal images were captured at various time points using a thermal camera.

For the study of photo-thermal-metabolic therapy, CT26 tumor-bearing BALB/c mice were allocated into 5 groups: Ctrl, NIR, B/T-HM, T-HM+NIR, and B/T-HM+NIR (with each mouse receiving B/T-HM: 250 μL, 2 mg/mL, 3BrPA: 0.5 mg/mL, and subjected to NIR irradiation: 0.5 w/cm^2 for 5 min) once tumors reached a volume of 80 mm^3. Following this, mice received *i.v.* injections of the specified treatments, with NIR exposure occurring 48 h later. Tumor volume were monitored and recorded bi-daily. In the investigation of photothermal-metabolic immunotherapy, tumors bearing mice were systematically grouped into 4 groups (G1: Ctrl, G2: B/T-HM+αPD-1, G3: T-HM+NIR+αPD-1, G4: B/T-HM+NIR+αPD-1, with the treatment formulation being B/T-HM: 250 μL, 2 mg/mL, 3BrPA: 0.5 mg/mL, NIR: 0.5 w/cm^2 for 5 min, and αPD-1: 20 μg per mouse) when tumor size achieved 80 mm^3. Subsequently, these mice were *i.v.* administered the respective compounds, followed by NIR irradiation after 48 h. Measurements of tumor growth were conducted every other day to evaluate the effects.

Statistical Analysis

In this study, all data are presented as mean±standard deviation (SD). Differences among groups were evaluated using both Analysis of Variance (ANOVA) and Student's *t*-test. Statistical analyses were performed using Graph Pad Prism version 9.5 and Excel 2016. A P-value less than 0.05 was deemed statistically significant.

Results and Discussion

Construction and Evaluation of Photo-Thermally Controllable Drug Delivery Platform

To precisely regulate tumor cell metabolism and reshape the tumor immune microenvironment to enhance tumor immunotherapy, we have developed a photo-thermally controllable drug delivery platform based on HPB and 1-tetradecanol, which has a phase transition temperature of 38°C. As depicted in Figure 1a, we initially synthesized Prussian Blue via a hydrothermal method, followed by etching with 0.01 M HCl to obtain HPB. Subsequently, at 85°C, 3-BrPA and 1-tetradecanol were mixed uniformly with HPB and then rinsed with deionized water to cool 25°C. The temperature change facilitated the transition of 1-tetradecanol from liquid to solid, encapsulating 3-BrPA within HPB to form B/T-HPB. Theoretically, HPB possesses excellent photo-thermal properties, allowing controlled release of 3-BrPA upon irradiate to an 808 nm laser when the temperature of B/T-HPB exceeds 38°C. Transmission electron microscopy (TEM) in Figure S1 reveals that the synthesized Prussian Blue had an initial size of approximately 180 nm, which slightly reduced to about 120 nm after HCl etching (Figure 1b). Further, the characteristic absorption peak of 3-BrPA in B/T-HPB was identified using a UV spectrophotometer, indicating successful encapsulation of 3-BrPA by 1-tetradecanol within HPB (Figure 1c). The element mapping and energy spectrum of B/T-HM also support the aforementioned conclusions (Figure S2). To enhance the in vivo circulation and tumor targeting of B/T-HPB, tumor cell membranes were used to physically extrude and modify it, resulting in B/T-HM as demonstrated by SDS-PAGE in Figure S3, confirming successful membrane modification on B/T-HPB. After membrane modification, the zeta potential of B/T-HM became more negative, which could favor its circulation and drug delivery in vivo (Figure 1d). Dynamic light scattering (DLS) further analyzed the hydrodynamic radius of PB, HPB, B/T-HPB, and B/T-HM, correlating with TEM results, showing that drug loading and membrane modification had minimal impact on their sizes

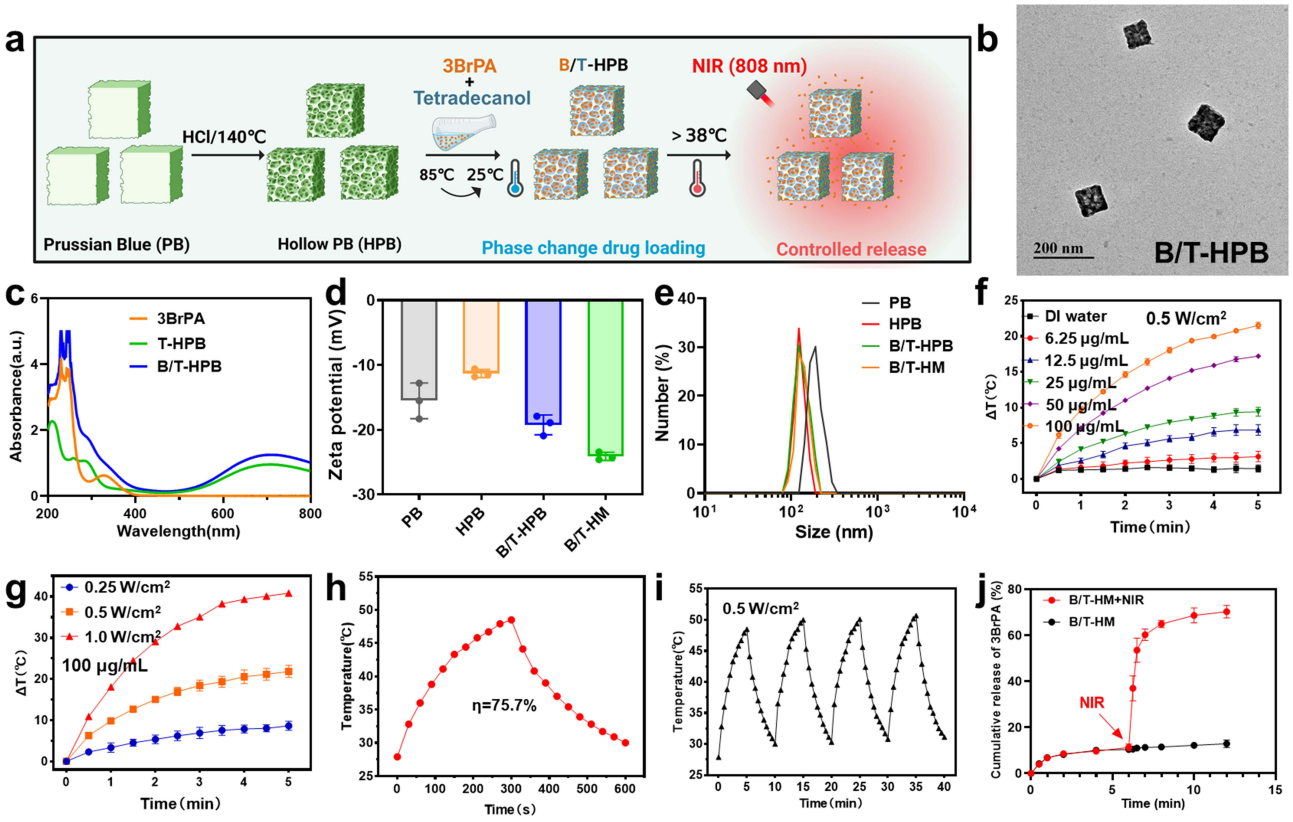

Figure 1 (**a**) The schematic diagram of the preparation of Hollow Prussian Blue (HPB) encapsulating 3-bromopyruvate (3BrPA) with phase change 1-tetramanol (B/T-HPB) and the principle of photothermal controlled release. (**b**) TEM image of B/T-HPB. (**c**) The UV spectra of 3BrPA, T-HPB, and B/T-HPB. (**d**) Zeta potential of PB, HPB, B/T-HPB and tumor cell membrane modified B/T-HPB (B/T-HM). (**e**) DLS of PB, HPB, B/T-HPB and B/T-HM. (**f**) Temperature changes of B/T-HM at different concentrations (HPB: 6.25~100 μg/mL) under 808 nm near-infrared (NIR) light irradiation (with a light power density of 0.5 W/cm^2). (**g**) Temperature change curves of B/T-HM (1.0 mL, HPB: 100 μg/mL) under NIR light irradiation at different power density. (**h**) Photothermal conversion efficiency (η) of B/T-HM (HPB: 100 μg/mL). (**i**) Temperature evolution of B/T-HM over 4 LASER ON/OFF cycles of 808 nm NIR laser irradiation (0.5 W/cm^2). (**j**) 3BrPA controlled release curves in B/T-HM with or without 808 nm NIR irradiation (0.5 W/cm^2, 5 min). Error bars represent mean ± s.d. (n=3).

(Figure 1e). Following this, to clarify the drug release capability of B/T-HPB under 808 nm light, we first evaluated the photo-thermal performance of B/T-HM. As shown in Figure 1f, under 0.5 W/cm^2 of 808 nm light for 5 minutes, the temperature of the solution increased more as the HPB content increased (6.25~100 μg/mL), exceeding 20°C when the HPB concentration reached 100 μg/mL, which was also indicated by the photothermal photos of B/T-HM (Figure S4). Additionally, under varying irradiation powers, B/T-HM still demonstrated good photo-thermal performance, achieving a photo-thermal conversion efficiency of 75.7% (Figure 1g and h). Notably, the photo-thermal performance of B/T-HM showed no significant loss even under repeated on/off cycles of irradiation (Figure 1i). Finally, the cumulative drug release curve confirmed that approximately 70.3±2.73% of 3-BrPA could be released from B/T-HM under 0.5 W/cm^2 of 808 nm light after 5 min of irradiation. Without irradiation, the cumulative release of 3BrPA from B/T-HM was only 12.9±1.65% (Figure 1j). These results illustrate the successful construction of a photo-thermally controllable drug delivery platform encapsulating 3-BrPA, capable of specifically releasing the drug under light conditions of 0.5 W/cm^2 at 808 nm, providing a solid theoretical and experimental foundation for subsequent cellular level and in vivo tumor treatment, and precise regulation of tumor cell metabolism to reshape the tumor immune microenvironment.

Cellular-Level Regulation of Photo-Thermally Activated B/T-HM

After evaluating the excellent drug-loading and photo-thermal-controlled release capabilities of B/T-HM, we further verified its regulatory effects and efficacy on tumor cells under light-controlled conditions at the cellular level. Initially, T-HM was co-incubated with HUVEC cells and was found to exhibit no significant cytotoxicity even at concentrations exceeding 200 μg/mL (Figure S5). Subsequently, B/T-HM was co-incubated with CT26 cells, where it was efficiently endocytosed. Confocal images show significant intracellular FITC-B/T-HM signals at 6 hours, possibly due to the homotypic targeting of the tumor cell membrane (Figure 2a). Notably, through lysosomal co-localization staining, as shown in Figure S6, B/T-HM can also escape from lysosomes within the cells, setting the stage for intracellular release of 3-BrPA and its impact on tumor cell metabolism. 3-BrPA, a hexokinase II (HK2) inhibitor, primarily regulates tumor cell metabolism by inhibiting HK2 activity, hence the HK2 activity in CT26 cells treated with B/T-HM and 808 nm NIR irradiation was measured using an HK2 activity assay kit. As shown in Figure 2b, B/T-HM slightly inhibits HK2 activity, with significant inhibition observed upon release of 3-BrPA under 808 nm light exposure. Additionally, the effective action of 3-BrPA also reduces the gene and protein expression levels of HK2 through its inhibition of the glycolysis pathway (Figure 2c). Furthermore, high levels of glycolysis are also associated with increased PD-L1 expression on tumor cell surfaces, which promotes immune evasion. Theoretically, inhibiting tumor cell glycolysis could reduce PD-L1 expression. Western blot analysis of tumor cells treated with B/T-HM, T-HM+NIR, and B/T-HM+NIR showed a significant reduction in PD-L1 expression following B/T-HM+NIR treatment compared to B/T-HM and T-HM+NIR (Figure 2d), benefiting subsequent T-cell-mediated anti-tumor immune responses. For another, as lactate, the final product of glycolysis, further acidifies the tumor microenvironment, reducing T-cell activity, effective restriction of tumor cell glycolysis by B/T-HM+NIR leads to decreased lactate production, providing a conducive environment for T-cell anti-tumor functions. To confirm this, lactate levels in the culture medium of CT26 cells from the respective treatment groups were measured using a lactate assay kit, revealing that photo-thermally promoted release of 3-BrPA by B/T-HM could reduce lactate content to 2.04±0.47% (Figure 2e). Subsequently, the cytotoxicity of B/T-HM combined with photo-thermal therapy on tumor cells was assessed using a CCK-8 assay kit. Compared to free 3-BrPA, B/T-HM enhanced the safety of 3-BrPA, possibly due to the drug encapsulation capabilities of 1-tetradecanol. T-HM combined with 808 nm NIR irradiation killed over 50% of tumor cells, and encapsulation of 3-BrPA with B/T-HM+NIR led to the killing of about 90% of tumor cells (Figures 2f and S7). Finally, using Western blot, key proteins related to ICD such as HSP70 and HSP90 were found to be significantly elevated in tumor cells treated with B/T-HM +NIR, and an increase in ATP content was also detected in the medium by ATP assay kits (Figure 2g and h). These results indicate that photo-thermally activated B/T-HM not only effectively inhibits tumor cell glycolysis via the HK2 pathway but also reduces PD-L1 expression and lactate production. Simultaneously, the photo-thermal-mediated B/T-HM synergistic treatment effectively kills tumor cells while inducing ICD, providing reliable cellular-level validation for the efficacy of subsequent T-cell function and enhancement of immunotherapy.

In vivo Effects and Anti-Tumor Evaluation of Photothermally Controllable B/T-HM

After validating the cellular-level functions of the photo-thermally controllable B/T-HM, its behavior and effects in vivo were further evaluated. Initially, DiD-labeled B/T-HM was administered intravenously into CT26 tumor-bearing mice, and the

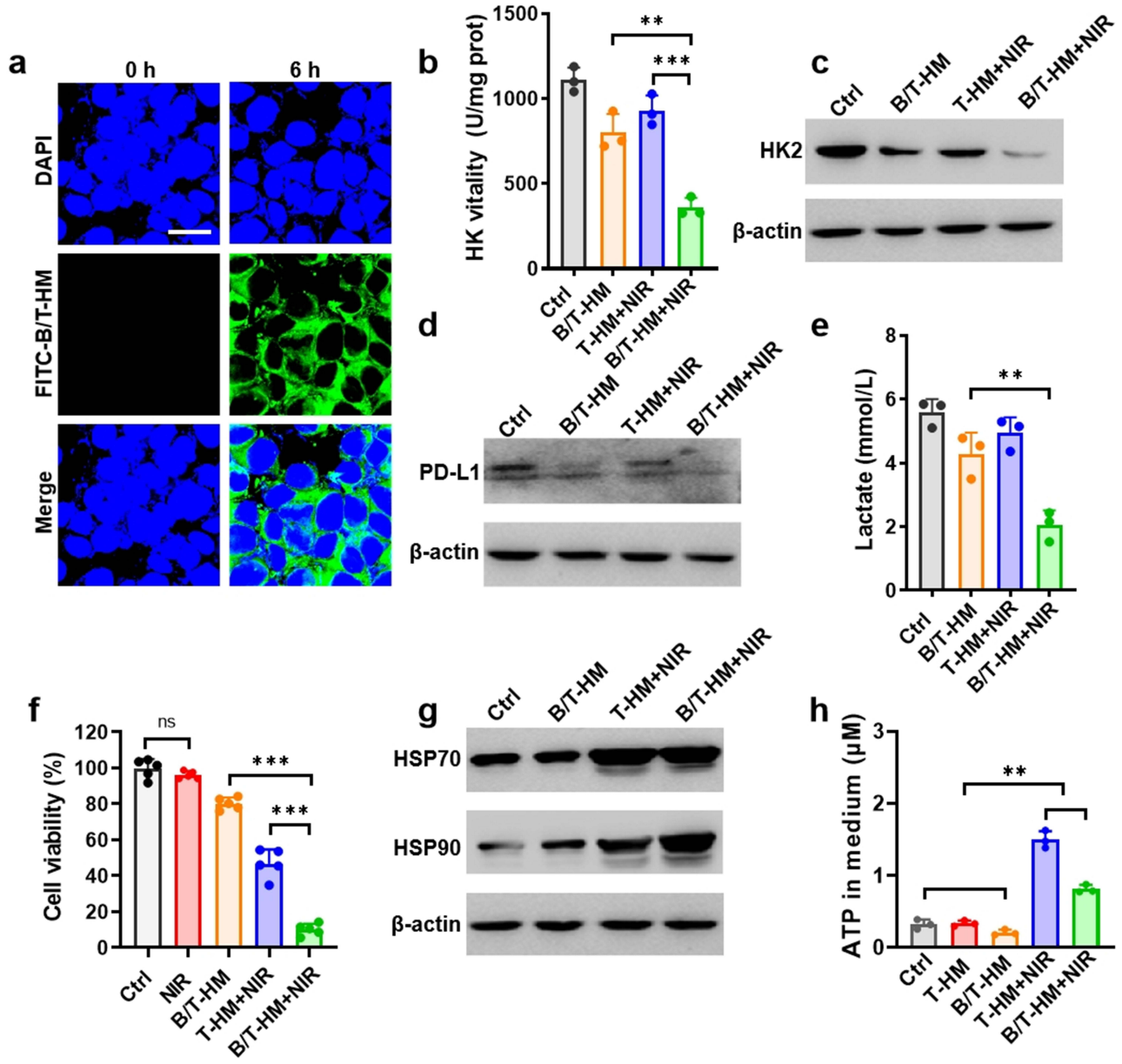

Figure 2 (**a**) Confocal images of FITC labeled B/T-HM phagocytosed by CT26 tumor cells (scale bar: 10 μm). (**b**) Hexokinase 2 (HK2) vitality in CT26 cells treated with B/T-HM, T-HM+NIR and B/T-HM+NIR. (**c**) Western blot analysis of HK2 expression levels in CT26 cells treated with B/T-HM, T-HM+NIR and B/T-HM+NIR. (**d**) Western blot analysis of PD-L1 expression on CT26 cells treated with B/T-HM, T-HM+NIR and B/T-HM+NIR. (**e**) Lactate content in the medium of CT26 cells treated with B/T-HM, T-HM+NIR, and B/T-HM +NIR. (**f**) Cell viability of CT26 cells treated with B/T-HM, T-HM+NIR and B/T-HM+NIR. (**g**) Western blot analysis of HSP70 and HSP90 expression levels in CT26 cells treated with B/T-HM, T-HM+NIR and B/T-HM+NIR. (**h**) ATP content in the medium of CT26 cells treated with B/T-HM, T-HM+NIR, and B/T-HM+NIR. (HPB: 100 μg/mL, 3BrPA: 25 μg/mL, NIR: 0.5 W/cm^2, 5 min). Error bars represent mean ± s.d. (n=3). P values in (**c, d, f** and **h**) were calculated by one-way ANOVA test. (**P < 0.01, ***P < 0.001).

distribution of DiD-B/T-HM within the body was tracked at different time points by the IVIS imaging system. As shown in Figure 3a, over time, DiD-B/T-HM gradually accumulated at the tumor site, reaching peak levels between 24 and 48 h post-injection. This indicates that the tumor cell membrane-modified B/T-HM could efficiently reach the tumor site through EPR effect and homotypic targeting, laying a foundation for its functional deployment at the tumor site. Concurrently, the specific distribution of B/T-HM in organs and tumors was analyzed by ICP by detecting Fe content; 24 h post-injection, the B/T-HM content in the tumor reached 9.64±0.84% ID/g, and even higher at 12.44±1.99% ID/g after 48 h. These results are consistent with those from the IVIS imaging, indicating a high tumor enrichment efficiency of B/T-HM, while its content in normal organs gradually decreased due to metabolism (Figure 3b). Subsequently, the efficacy of B/T-HM in the tumor was assessed through photo-thermal imaging 48 h post-injection. As illustrated in Figure 3c, over the course of irradiation, relative to the PBS group, B/

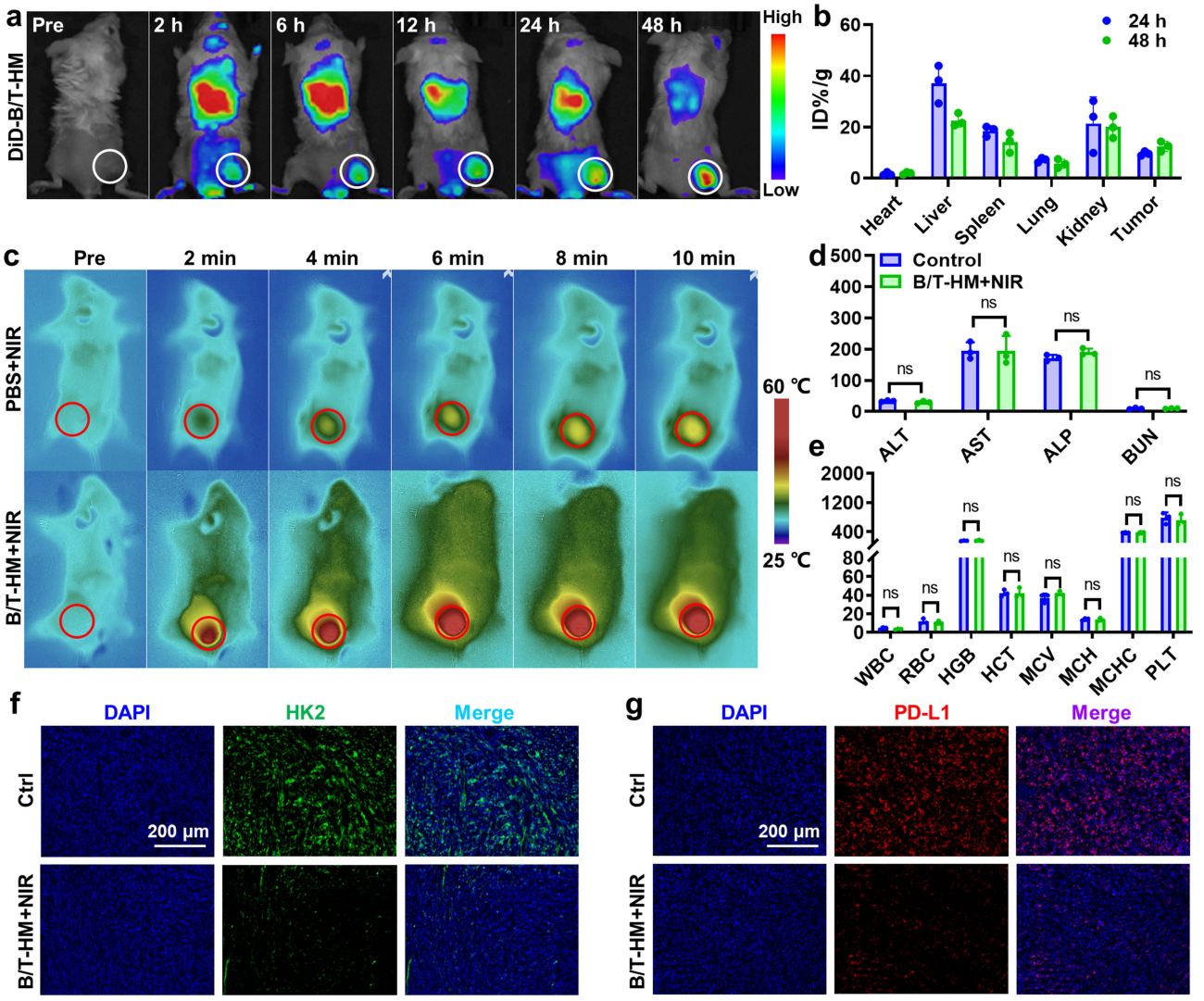

Figure 3 (**a**) IVIS fluorescence imaging of DiD labeled B/T-HM in CT26 tumor-bearing mice after *i.v.* injection at different time points. (**b**) Biodistribution of B/T-HM at different time points after *i.v.* injection. Error bars represent mean ± s.d. (n=3). (**c**) Photothermal imaging of CT26 tumor-bearing mice after different durations of 808 nm NIR light irradiation after *i.v.* injection with B/T-HM for 48 h (NIR: 0.5 W/cm^2). (**d**) Blood biochemistry (ALT (U/L), AST (U/L), ALP (U/L), BUN (mmol/L)) and (**e**) blood routine (WBC (10^9/L), RBC (10^{12}/L), HGB (g/L), HCT (%), MCV (fL), MCH (pg), MCHC (g/L), PLT(10^9/L)) analysis of mice post 21 days *i.v.* injection with B/T-HM. Error bars represent mean ± s.d. (n=3). (**f**) Immunofluorescence images of HK2 expression in CT26 tumors treated with B/T-HM+NIR (green: HK2$^+$) (**g**) Immunofluorescence images of PD-L1 expression in CT26 tumors treated with B/T-HM+NIR (red: PD-L1$^+$) (100 μL B/T-HM, 3BrPA: 6.25 mg/kg, NIR: 0.5 W/cm^2, 5 min). P values in (**d** and **e**) were calculated by Student's *t*-test. (ns P> 0.05).

T-HM could raise the tumor tissue temperature to above 50°C within 6 minutes of 808 nm NIR irradiation, ensuring the in vivo release of 3-BrPA and facilitating synergistic photo-thermal therapy of the tumor. Notably, the *i.v.* injection of B/T-HM appeared to have no significant impact on the health of the mice, as evidenced by the blood biochemistry (ALT, AST, ALP, BUN) and blood routine (WBC, RBC, HGB, HCT, MCV, MCH, MCHC, PLT) analyses 21 days post-injection (Figure 3d and e) and the H&E staining of organs (Figure S8), which showed no significant differences compared to the control group. Following this, tumor tissues from mice treated with B/T-HM+NIR underwent immunofluorescence histological analysis, demonstrating significant reductions in the expression levels of HK2 (green fluorescence) and PD-L1 (red fluorescence) in tumor tissues, indicating that the photo-thermally controllable B/T-HM can indeed regulate tumor metabolism in vivo (Figure 3f and g).

To verify the photo-thermal-metabolic antitumor effects of photo-thermally controllable B/T-HM in vivo, a subcutaneous CT26 tumor model in mice was established. Once the tumor volume approached ~80 mm^3, the mice were randomly assigned to 5 different groups (Ctrl, NIR, B/T-HM, T-HM+NIR, and B/T-HM+NIR). On day 0, the respective formulations were administered, followed by 808 nm NIR irradiation on day 2. The mice's growth curves were monitored and analyzed subsequently (Figure 4a). As illustrated in Figure 4b, compared to the Ctrl group, B/T-HM exhibited a mild therapeutic

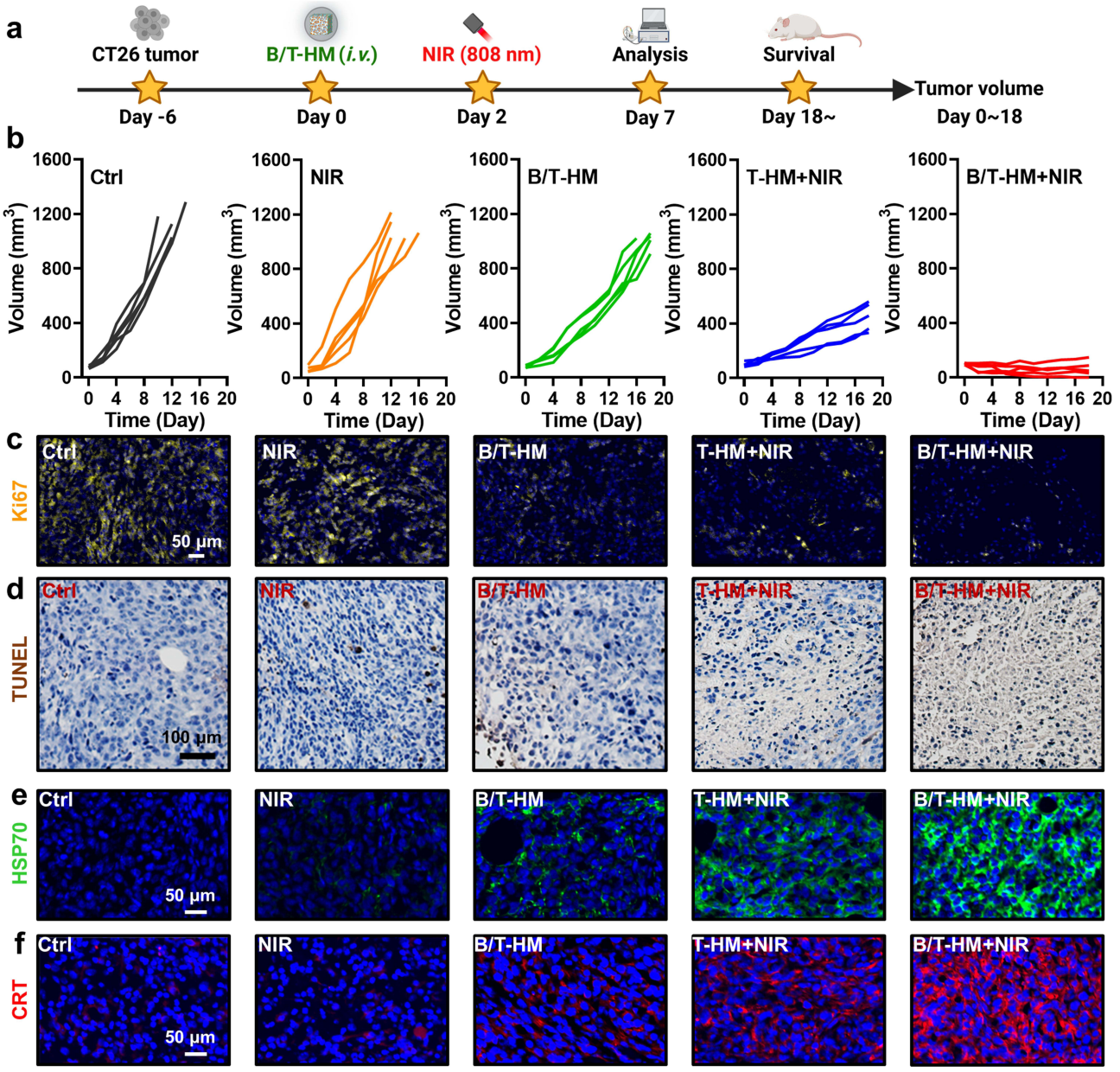

Figure 4 (**a**) Schematic diagram of controlled photothermal-metabolic therapy mediated by B/T-HM. (**b**) CT26 tumors growth curves after treated with NIR, B/T-HM, T-HM +NIR and B/T-HM+NIR (100 μL B/T-HM, 3BrPA: 6.25 mg/kg, NIR: 0.5 W/cm^2, 5 min) (n=5). (**c**) Confocal microscopy images of Ki67 (yellow) expression in tumor tissues at day 7 post treatments. (**d**) Confocal microscopy images of TUNEL (brown) in tumor tissues at day 7 post treatments. (**e**) Confocal microscopy images of HSP70 (green) expression in tumor tissues at day 7 post treatments. (**f**) Confocal microscopy images of CRT (red) expression in tumor tissues at day 7 post treatments.

effect, likely due to partial release of 3-BrPA at the tumor site. The T-HM+NIR group, benefiting from HPB's excellent photo-thermal properties, demonstrated a better photo-thermal therapeutic effect on tumors. Most notably, the photo-thermal-metabolic antitumor effect of photo-thermally controllable B/T-HM (B/T-HM+NIR) effectively halted tumor growth and prolonged the mice's survival to beyond 30 days, all while being safe and effective, with no significant weight loss observed in the mice (Figures S9 and S10). Since 3-BrPA can inhibit tumor proliferation by suppressing glycolysis in tumor cells, Ki67 immunofluorescence staining (yellow) was performed on tumor tissues on day 7 post-treatment to assess tumor cell proliferation. The results showed a significant reduction in Ki67 fluorescence in the tumors treated with B/T-HM+NIR, indicating a substantial suppression of tumor proliferation (Figure 4c). Furthermore, the photo-thermal-metabolic treatment mediated by B/T-HM+NIR also induced more apoptosis in tumor cells (Figure 4d). It is worth mentioning that previous

cellular-level validation showed that B/T-HM+NIR treatment led to the release of antigens associated with ICD in tumor cells. Therefore, the same validation was conducted at the animal treatment level, as shown in Figure 4e and f, where tumor tissues treated with B/T-HM+NIR exhibited increased expression and release of HSP70 and calreticulin (CRT). Meanwhile, another key indicator of ICD, HMGB1, also showed significant release after the photothermal-metabolic therapy (Figure S11). These results suggest that the photo-thermal-metabolic treatment mediated by B/T-HM+NIR not only effectively suppresses tumor growth but also induces ICD in tumor cells, offering possibilities for subsequent combination with immunotherapy to eradicate tumors.

Photo-Thermally Controllable B/T-HM Mediated Metabolic-Immunotherapy

In previous experiments, B/T-HM under 808 nm NIR irradiation was not only demonstrated to generate effective photo-thermal effects in vivo but also to efficiently inhibit glycolysis in tumor cells via the HK2 pathway, reduce lactate production, and decrease tumor cell proliferation. Additionally, it degraded PD-L1 on tumors and, after combined tumor cell eradication, facilitated the production of ICD. These findings reveal the potential of B/T-HM in reversing tumor metabolism-mediated immunosuppressive microenvironments and promoting tumor immunotherapy. Reducing lactate production and promoting tumor PD-L1 degradation may further enhance the efficacy of T cells in tumor immunotherapy. To enhance its effectiveness, we combined B/T-HM+NIR with an anti-PD-1 antibody (αPD-1), which can block the PD-L1 /PD-1 pathway and further activate T cells, in a strategy termed photo-thermally controllable metabolic-immunotherapy to potentially eradicate tumors. As shown in Figure 5a, a CT26 tumor-bearing mouse model was established, and once the

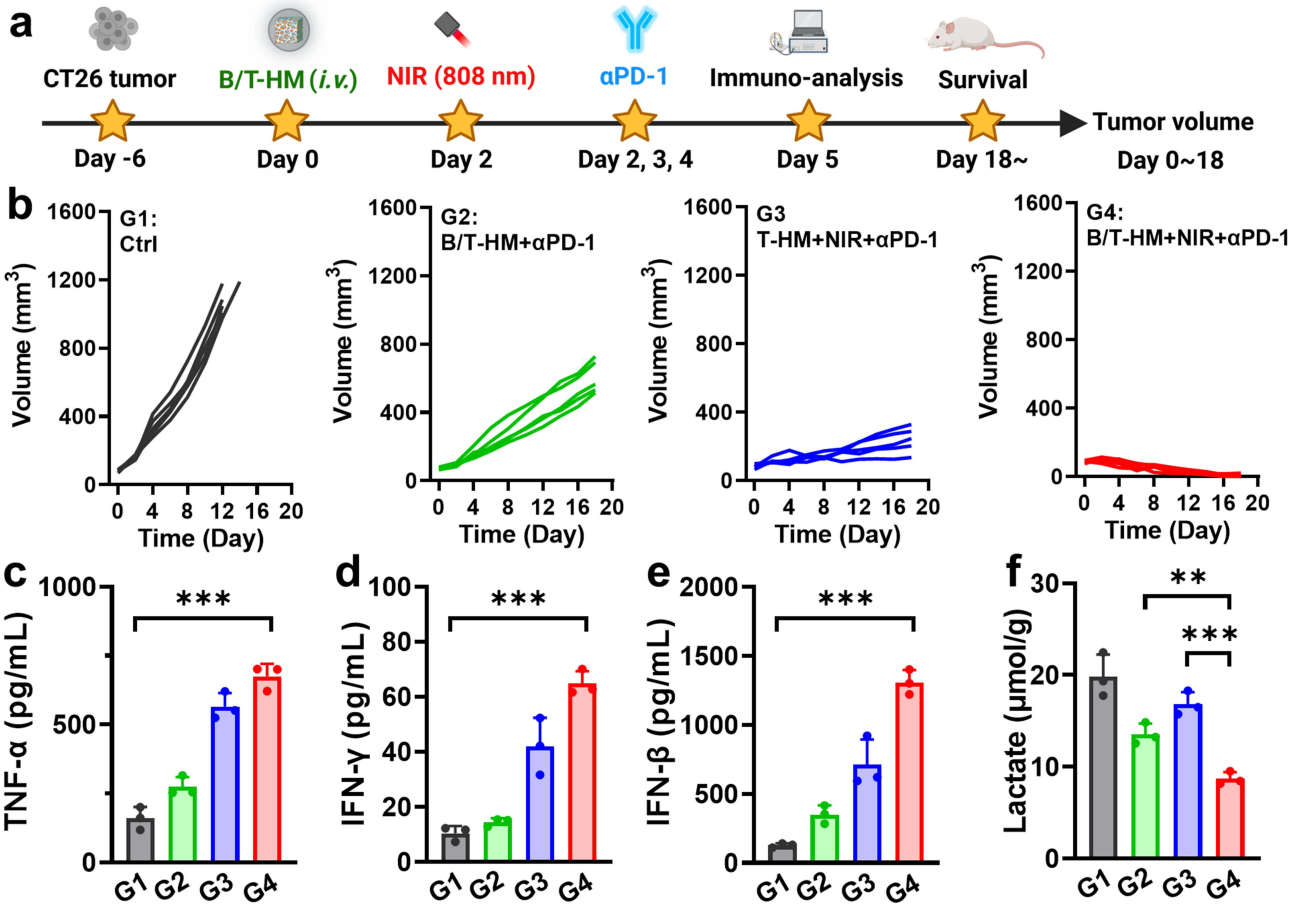

Figure 5 (**a**) Schematic diagram of photo-thermally controllable tumor metabolic modulation to enhance immunotherapy. (**b**) CT26 tumors growth curves of mice post controllable photothermal-metabolic immunotherapy (B/T-HM+αPD-1, T-HM+NIR+αPD-1 and B/T-HM+NIR+αPD-1). (n=5). (**c-e**) The levels of TNF-α (**c**), IFN-γ (**d**) and IFN-β (**e**) in tumor bearing mice serum at day 5 post treatments detected by ELISA kit. Error bars represent mean ± s.d. (n=3). (**f**) Lactate content in CT26 tumor tissues post treatments. P values in **c–f** were calculated by one-way ANOVA test. (**P < 0.01, ***P < 0.001).

tumor volume approached ~80 mm^3, the mice were randomly assigned to 4 different groups (Ctrl, B/T-HM+αPD-1, T-HM +NIR+αPD-1, and B/T-HM+NIR+αPD-1), and treated accordingly. Compared to the groups not combined with αPD-1 for immunotherapy, the B/T-HM+NIR+αPD-1 group could nearly completely eliminate the tumors (Figure 5b). After the photo-thermally controllable metabolic-immunotherapy, 80% of the mice survived more than 60 days without significant impact on their health (Figures S12 and S13). To assess the mechanism of action of this treatment, we first evaluated anti-tumor related cytokines such as TNF-α, IFN-γ, and IFN-β in the serum of mice using an ELISA kit on day five post-treatment. As Figure 5c–e show, compared to the Ctrl, B/T-HM+αPD-1, and T-HM+NIR+αPD-1 groups, the concentrations of these cytokines were markedly elevated in the B/T-HM+NIR+αPD-1 group, with the rise in IFN-β suggesting possible activation of NK cells. Further, before assessing changes in T cell phenotypes and proportions within the tumor micro-environment, the lactate content in the tumor tissues of each group was measured using a lactate assay kit. Results indicated a slight reduction in the B/T-HM+αPD-1 group and a significant reduction in the B/T-HM+NIR+αPD-1 group, which would be more conducive to subsequent T cell infiltration and activation (Figure 5f). Subsequently, through flow cytometry, we assessed the maturity ratio of dendritic cells (DCs) in lymph nodes, a crucial step for activating tumor-specific T cells. The metabolic-immunotherapy mediated by B/T-HM+NIR+αPD-1 also aided in the activation of DC cells, elevating the $CD11c^+CD80^+CD86^+$ DC cell maturity ratio from 14.99±5.64% in the control group to 37.97±1.50% (Figure 6a and b). Concurrently, the proportion of infiltrating $CD3^+CD8^+$ T cells in the tumor increased to 42.4±1.66%, while the $CD3^+CD4^+$ T cell ratio showed no significant change (Figure 6c and d). To further refine the $CD8^+$ T cell phenotype, flow cytometry characterization revealed that the majority of the increased $CD3^+CD8^+$ T cells were IFN-γ^+ CD8 T cells and Granzyme B^+

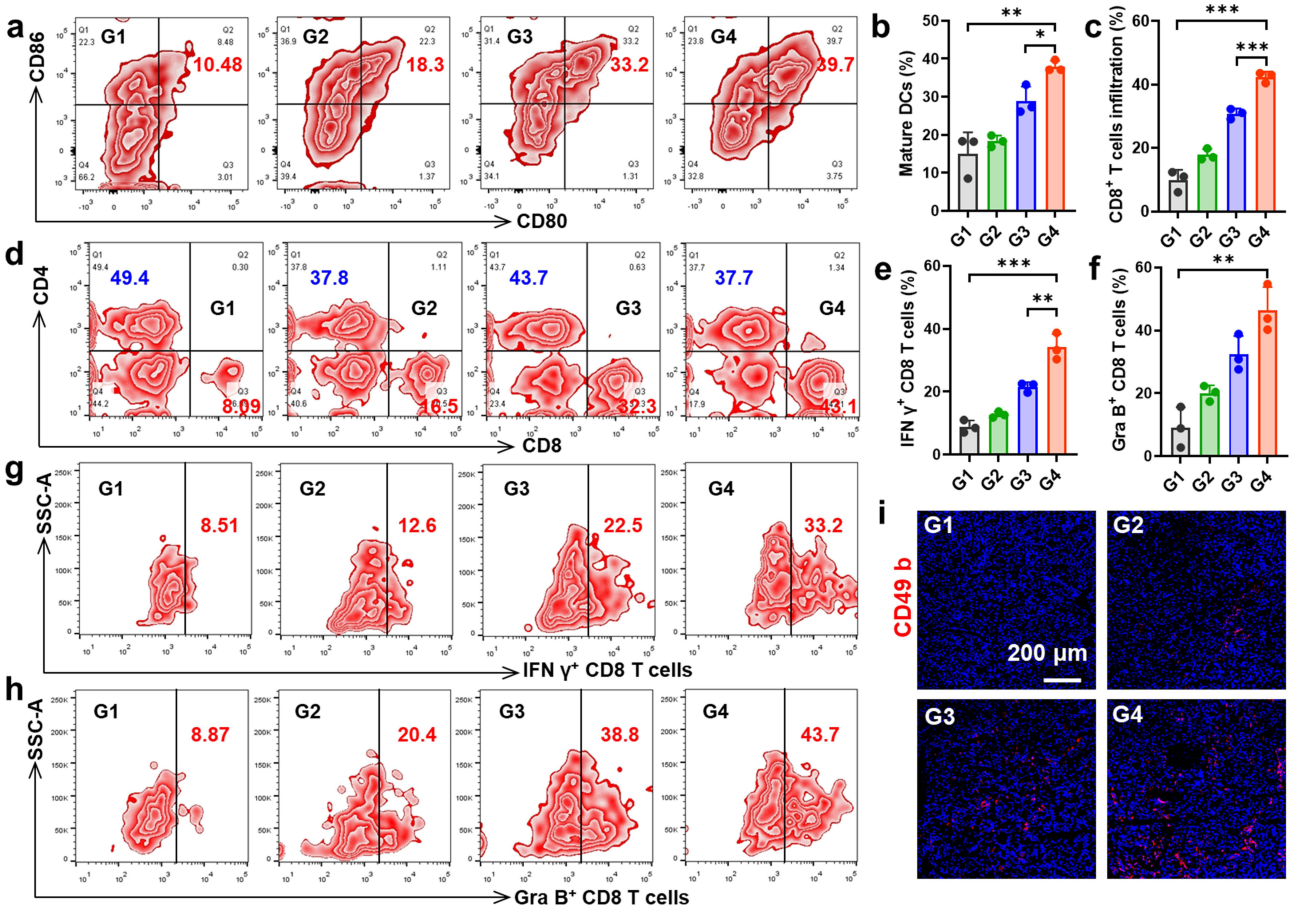

Figure 6 (**a** and **b**) Representative FACS plots (**a**) and statistical analysis (**b**) of DC maturation at day 5 post treatments. Error bars represent mean ± s.d. (n=3). (**c** and **d**) Statistical analysis (**c**) and representative FACS plots (**d**) of T cells at day 5 post treatments. Error bars represent mean ± s.d. (n=3). (**e-h**) FACS statistical analysis and representative FACS plots of IFN-γ^+CD8^+ T cells (**e** and **g**) and Granzyme B^+CD8^+ T cells (**f** and **h**) infiltrate in CT26 tumors post treatments. Error bars represent mean ± s.d. (n=3). (**i**) Confocal microscopy images of NK cells (red) infiltrate in tumor tissues at day 5 post treatments. P values in (**b, c, e** and **f**) were calculated by one-way ANOVA test. (*P < 0.05, **P < 0.01, ***P < 0.001).

CD8 T cells, the two main anti-tumor $CD8^+$ T cell phenotypes (Figure 6e–h). Notably, immuno-fluorescent staining of the tumor tissues also found an increase in infiltrating NK cells with the progression of treatment, consistent with the earlier rise in IFN-β (Figure 6i). Thus, B/T-HM under 808 nm NIR irradiation combined with αPD-1 can effectively reverse the tumor metabolism-mediated immunosuppressive environment and activate the immune cycle, promoting tumor metabolic-immunotherapy to eliminate the tumor.

Conclusion

This study aims to address the changes in the TME caused by the unique metabolic ways of tumor cells, which limit the effectiveness of tumor immunotherapy, particularly the function of T cells. To reverse the immunosuppressive microenvironment caused by tumor cell glycolysis and to promote metabolic-immune therapy for cancer, we have designed and developed a novel photo-thermally controllable drug delivery platform (B/T-HM). This platform consists of hollow mesoporous Prussian blue nanoparticles, whose surface is modified with tumor cell membranes and encapsulates a drug known as 3-BrPA. It can achieve photo-thermally controllable release and delivery through a phase change material, 1-tetradecanol, thus precisely regulating tumor cell glycolysis metabolism, and is expected to boost the effectiveness of tumor immunotherapy. In vitro, B/T-HM demonstrated excellent photo-thermal performance and drug encapsulation ability, precisely releasing 3-BrPA under 808 nm NIR irradiation. After being internalized by tumor cells, B/T-HM can inhibit tumor cell glycolysis and proliferation through the HK2 pathway under NIR irradiation, reduce lactate production and PD-L1 expression, effectively kill tumor cells and release TAA after synergistic photo-thermal therapy. In vivo, B/T-HM can target and accumulate in tumors, significantly inhibit tumor proliferation and ICD under photo-thermal synergistic control, while reversing the immune-suppressive microenvironment caused by tumor metabolism-induced PD-L1 upregulation and acid production, providing a conducive immune microenvironment for T cell infiltration and activation. When combined with αPD-1, B/T-HM-mediated photo-thermally controllable metabolic-immune therapy can effectively eradicate tumors. Overall, our study utilizes photo-thermal therapy to precisely regulate tumor cell metabolism, further improving the tumor immune-suppressive microenvironment. This strategy provides a novel perspective for effectively combining photo-thermal therapy, metabolic regulation, and immunotherapy, opening new avenues for cancer treatment research.

Ethics Approval and Consent to Participate

All animal studies were approved by the Animal Ethics and Welfare Committee of Nanjing Medical University.

Acknowledgments

This work was partially supported by the China Postdoctoral Science Foundation (2023M741796) and the Postdoctoral research program of Taizhou Clinical Medicine School of Nanjing Medical University (TZBSHKY202204), Shanxi Province 136 Revitalization Medical Project Construction Funds, general Program of Shanxi Province Basic Research (Free Exploration, 202303021221189).

Disclosure

The authors declare no conflict of interests in this work.

References

1. Martin JD, Cabral H, Stylianopoulos T, Jain RK. Improving cancer immunotherapy using nanomedicines: progress, opportunities and challenges. *Nat Rev Clin Oncol*. 2020;17(4):251–266. doi:10.1038/s41571-019-0308-z
2. Xue LL, Thatte AS, Mai D, et al. Responsive biomaterials: optimizing control of cancer immunotherapy. *Nat Rev Mater*. 2024;9(2):100–118. doi:10.1038/s41578-023-00617-2
3. Du S, Yan J, Xue Y, Zhong Y, Dong Y. Adoptive cell therapy for cancer treatment. *Exploration*. 2023;3(4):20210058. doi:10.1002/EXP.20210058
4. Kumagai S, Itahashi K, Nishikawa H. Regulatory T cell-mediated immunosuppression orchestrated by cancer: towards an immuno-genomic paradigm for precision medicine. *Nature Reviews Clinical Oncology*. 2024;21(4):294–311. doi:10.1038/s41571-024-00870-6
5. Lu Q, Kou DQ, Lou SH, et al. Nanoparticles in tumor microenvironment remodeling and cancer immunotherapy. *J Hematol Oncol*. 2024;17(1):16. doi:10.1186/s13045-024-01535-8
6. Ding Y, Wang Y, Hu Q. Recent advances in overcoming barriers to cell-based delivery systems for cancer immunotherapy. *Exploration*. 2022;2(3):20210106. doi:10.1002/EXP.20210106

7. Kumagai S, Koyama S, Itahashi K, et al. Lactic acid promotes PD-1 expression in regulatory T cells in highly glycolytic tumor microenvironments. *Cancer Cell*. 2022;40(2):201–218. doi:10.1016/j.ccell.2022.01.001
8. Qiao QQ, Hu SF, Wang X. The regulatory roles and clinical significance of glycolysis in tumor. *Cancer Commun*. 2024;44(7):761–786. doi:10.1002/cac2.12549
9. Reinfeld BI, Rathmell WK, Kim TK, Rathmell JC. The therapeutic implications of immunosuppressive tumor aerobic glycolysis. *Cell. Mol. Immunol.* 2022;19(1):46–58. doi:10.1038/s41423-021-00727-3
10. Peng JH, Cui YY, Xu SP, et al. Altered glycolysis results in drug-resistant in clinical tumor therapy. *Oncol Lett*. 2021;21(5). doi:10.3892/ol.2021.12630
11. Apostolova P, Pearce EL. Lactic acid and lactate: revisiting the physiological roles in the tumor microenvironment. *Trends Immunol*. 2022;43(12):969–977. doi:10.1016/j.it.2022.10.005
12. DePeaux K, Delgoffe GM. Metabolic barriers to cancer immunotherapy. *Nat Rev Immunol*. 2021;21(12):785–797. doi:10.1038/s41577-021-00541-y
13. Kooshki L, Mahdavi P, Fakhri S, Akkol EK, Khan H. Targeting lactate metabolism and glycolytic pathways in the tumor microenvironment by natural products: a promising strategy in combating cancer. *Biofactors*. 2022;48(2):359–383. doi:10.1002/biof.1799
14. Elia I, Rowe JH, Johnson S, et al. Tumor cells dictate anti-tumor immune responses by altering pyruvate utilization and succinate signaling in CD8 T cells. *Cell Metab.* 2022;34(8):1137–1150. doi:10.1016/j.cmet.2022.06.008
15. Quinn WJ, Jiao J, TeSlaa T, et al. Lactate limits T cell proliferation via the NAD(H) redox state. *Cell Rep*. 2020;33(11):108500. doi:10.1016/j.celrep.2020.108500
16. Wang K, Zhang Y, Chen ZN. Metabolic interaction: tumor-derived lactate inhibiting CD8 T cell cytotoxicity in a novel route. *Signal Transduction Tar*. 2023;8(1):52. doi:10.1038/s41392-023-01320-y
17. Watson MJ, Vignali PDA, Mullett SJ, et al. Metabolic support of tumour-infiltrating regulatory T cells by lactic acid. *Nature*. 2021;591(7851):7851):645–651. doi:10.1038/s41586-020-03045-2
18. Guo D, Tong Y, Jiang X, et al. Aerobic glycolysis promotes tumor immune evasion by hexokinase2-mediated phosphorylation of IkappaBalpha. *Cell Metab*. 2022;34(9):1312–1324e6. doi:10.1016/j.cmet.2022.08.002
19. He H, Xiao L, Wang J, Guo D, Lu Z. Aerobic glycolysis promotes tumor immune evasion and tumor cell stemness through the noncanonical function of hexokinase 2. *Cancer Commun*. 2023;43(3):387–390. doi:10.1002/cac2.12404
20. Zhang R, Yang Y, Dong W, et al. D-mannose facilitates immunotherapy and radiotherapy of triple-negative breast cancer via degradation of PD-L1. *Proc Natl Acad Sci U S A*. 2022;119(8):e2114851119. doi:10.1073/pnas.2114851119
21. Chelakkot C, Chelakkot VS, Shin Y, Song K. Modulating glycolysis to improve cancer therapy. *Int J Mol Sci*. 2023;24(3):2606. doi:10.3390/ijms24032606
22. Ciscato F, Ferrone L, Masgras I, Laquatra C, Rasola A. Hexokinase 2 in cancer: a prima donna playing multiple characters. *Int J Mol Sci*. 2021;22(9):4716. doi:10.3390/ijms22094716
23. Dai H, Fan Q, Wang C. Recent applications of immunomodulatory biomaterials for disease immunotherapy. *Exploration*. 2022;2(6):20210157. doi:10.1002/EXP.20210157
24. Li T, Guo L, Li J, et al. Precision USPIO-PEG-SLe(x) nanotheranostic agent targeted photothermal therapy for enhanced anti-PD-L1 immunotherapy to treat immunotherapy resistance. *Int J Nanomed*. 2024;19:1249–1272. doi:10.2147/IJN.S445879
25. Qi Z, Pei P, Zhang Y, et al. (131)I-alphaPD-L1 immobilized by bacterial cellulose for enhanced radio-immunotherapy of cancer. *J Control Release*. 2022;346:240–249. doi:10.1016/j.jconrel.2022.04.029
26. Zheng Y, Han Y, Sun Q, Li Z. Harnessing anti-tumor and tumor-tropism functions of macrophages via nanotechnology for tumor immunotherapy. *Exploration*. 2022;2(3):20210166. doi:10.1002/EXP.20210166
27. Huang Y. Targeting glycolysis for cancer therapy using drug delivery systems. *J Control Release*. 2023;353:650–662. doi:10.1016/j.jconrel.2022.12.003
28. Zhang L, Jiang C, Zhong Y, et al. STING is a cell-intrinsic metabolic checkpoint restricting aerobic glycolysis by targeting HK2. *Nat Cell Biol*. 2023;25(8):1208–1222. doi:10.1038/s41556-023-01185-x
29. Shen W, Liu T, Pei P, et al. Metabolic homeostasis-regulated nanoparticles for antibody-independent cancer radio-immunotherapy. *Adv Mater*. 2022;34(51):e2207343. doi:10.1002/adma.202207343
30. Liang JH, Wang C, Fan JL, et al. Hybrid membrane-camouflaged hollow prussian blue nanoparticles for shikonin loading and combined chemo/photothermal therapy of metastatic TNBC. *Mater Today Adv*. 2022;14:100215. doi:10.1016/j.mtadv.2022.100245
31. Lu L, Zhang C, Zou B, Wang Y. Hollow Prussian blue nanospheres for photothermal/chemo-synergistic therapy. *Int J Nanomed*. 2020;15:5165–5177. doi:10.2147/IJN.S252505
32. Wang XW, Cheng L. Multifunctional Prussian blue-based nanomaterials: preparation, modification, and theranostic applications. *Coordin Chem Rev*. 2020;419:213393. doi:10.1016/j.ccr.2020.213393
33. Zhu MZ, Wang P, Chen BQ, et al. Active-oxygenating hollow Prussian blue nanosystems loaded with biomacromolecules for photodynamic/photothermal therapy of cancer and alleviating hypoxic tumors. *Mater Design*. 2024;237:112618. doi:10.1016/j.matdes.2023.112618
34. Xu G, Li J, Zhang S, et al. Two-dimensional nano-biomaterials in regulating the tumor microenvironment for immunotherapy. *Nano Trans Med*. 2024;3:100045. doi:10.1016/j.ntm.2024.100045
35. Luo Y, He X, Du Q, et al. Metal-based smart nanosystems in cancer immunotherapy. *Exploration*;2024. 20230134. DOI:10.1002/EXP.20230134
36. Li H, Pei P, He Q, et al. Nanozyme-coated bacteria hitchhike on CD11b(+) immune cells to boost tumor radioimmunotherapy. *Adv Mater*. 2024;36(8):e2309332. doi:10.1002/adma.202309332
37. Shen WH, Han GH, Yu L, et al. Combined Prussian blue nanozyme carriers improve photodynamic therapy and effective interruption of tumor metastasis. *Int J Nanomed*. 2022;17:1397–1408. doi:10.2147/Ijn.S359156
38. Shi YH, Shi Y, Wang ZY, et al. Glucose-responsive mesoporous prussian blue nanoprobes coated with ultrasmall gold and manganese dioxide for magnetic resonance imaging and enhanced antitumor therapy. *Chem Eng J*. 2023;453:139885. doi:10.1016/j.cej.2022.139885
39. Xie YY, Zhang CH, Zhao Y, et al. Simultaneous modulation of hypoxia and metabolism in glioblastoma for enhanced radio-immunotherapy. *Adv Funct Mater*. 2024;34(12):2312197. doi:10.1002/adfm.202312197
40. Pei P, Wang Y, Shen W, et al. Oxygen-driven cuproptosis synergizes with radiotherapy to potentiate tumor immunotherapy. *Aggregate*. 2024;5(3):e484. doi:10.1002/agt2.484

41. Jin FY, Liu D, Xu XL, Ji JS, Du YZ. Nanomaterials-based photodynamic therapy with combined treatment improves antitumor efficacy through boosting immunogenic cell death. *Int J Nanomed*. 2021;16:4693–4712. doi:10.2147/Ijn.S314506
42. Li Y, Du ZK, Zhang Y, et al. Boosting theranostic performance of AIEgens using nanocatalyzer for robust cancer immunotherapy. *Adv Funct Mater*. 2024;34(23):2315127. doi:10.1002/adfm.202315127
43. Long Y, Fan J, Zhou N, et al. Biomimetic Prussian blue nanocomplexes for chemo-photothermal treatment of triple-negative breast cancer by enhancing ICD. *Biomaterials*. 2023;303:122369. doi:10.1016/j.biomaterials.2023.122369
44. He J, Song R, Xiao F, Wang M, Wen L. Cu(3)P/1-MT nanocomposites potentiated photothermal-immunotherapy. *Int J Nanomed*. 2023;18:3021–3033. doi:10.2147/IJN.S414117
45. Zare M, Mikkonen KS. Phase change materials for life science applications. *Adv Funct Mater*. 2023;33(12):2213455. doi:10.1002/adfm.202213455
46. Zhang CY, Li DD, Pei P, et al. Rod-based urchin-like hollow microspheres of BiS: facile synthesis, photo-controlled drug release for photoacoustic imaging and chemo-photothermal therapy of tumor ablation. *Biomaterials*. 2020;237:119835. doi:10.1016/j.biomaterials.2020.119835
47. Guo H, Guo M, Xia Z, Shao Z. Membrane-coated nanoparticles as a biomimetic targeted delivery system for tumour therapy. *Biomaterials Translational*. 2024;5(1):33–45. doi:10.12336/biomatertransl.2024.01.004